High-Frequency Behavior of the Dynamic Mobility and Dielectric Response of Concentrated Colloidal Dispersions

ARTICLE *in* LANGMUIR · SEPTEMBER 2009

Impact Factor: 4.46 · DOI: 10.1021/la9026255 · Source: PubMed

3 AUTHORS, INCLUDING:

Bronwyn H. Bradshaw-Hajek
University of South Australia
18 PUBLICATIONS **77** CITATIONS
SEE PROFILE

Stanley J Miklavcic
University of South Australia
91 PUBLICATIONS **1,148** CITATIONS
SEE PROFILE

Langmuir
Article
pubs.acs.org/Langmuir

High-Frequency Behavior of the Dynamic Mobility and Dielectric Response of Concentrated Colloidal Dispersions

B. H. Bradshaw-Hajek, S. J. Miklavcic,* and L. R. White

School of Mathematics and Statistics, University of South Australia, Mawson Lakes, SA 5082, Australia

Received July 17, 2009. Revised Manuscript Received August 20, 2009

A matched asymptotic analysis of the system of equations governing the electrokinetic cell model of ref 4 (Ahualli, S.; Delgado, A.; Miklavcic, S.; White, L. R. *Langmuir* **2006**, *22*, 7041) is performed. Asymptotic expressions are obtained for the dynamic mobility and complex conductivity response of a dense suspension of charged spherical particles to an applied electric field. The asymptotic expressions are compared with full numerical calculations of the linear response functions as a function of surface (ζ) potential, electrolyte strength, and particle density. We find that the numerical procedure used is robust and highly accurate at a very high frequency under a wide range of double-layer conditions. The asymptotic form for the dielectric response of the system is accurate to megahertz frequencies. The asymptotic formulas for the other response functions have limited viability as predictive tools within the current range of experimentally accessible frequencies but are useful as checks on numerical calculations.

1. Introduction

The dynamic mobility and complex conductivity are quantities that measure the dynamic response of a suspension of charged colloidal particles to the application of a time-dependent (oscillating) electric field. As such, these quantities have the potential to be used as inputs to quantitative pathways that determine colloidal properties such as mean particle size, surface potential, and surface charge. Moreover, the frequency, ω, dependence of the quantities is useful as a means of monitoring and analyzing particle interaction. What is required is a mechanism by which these experimentally accessible quantities can be related to the desired colloidal properties (charge, potential, size, particle interaction, etc.). One means of achieving this goal is through theoretical modeling, based on solving the set of fundamental electrokinetic equations: Navier−Stokes equations of hydrodynamics, ion conservation equations, Poisson equation for the electric potential, and ion transport equations.[1−6]

However, under highly concentrated conditions in which the particles interact strongly through electrical double-layer forces, there is considerable difficulty associated with solving the full system of equations. In a recent series of papers,[4−6] we and colleagues have formulated a rigorous cell model version of the electrokinetic problem for spherical particles of radius a that reduces the problem to solving the equations within a geometric cell surrounding an individual charged particle. The cell radius ($b = a\phi^{-1/3}$) depends on the volume fraction ϕ of particles present. Particle interactions are effected through application of self-consistent boundary conditions at the cell wall. This paper is based on this self-consistent, cell model approach. The use of the cell model to describe problems in electrokinetics is well-established,[7−15] although different candidate boundary conditions have been proposed.[4]

In our previous papers,[4−6,16] the system of governing equations, subject to the self-consistent boundary conditions, was solved numerically for a wide range of parameter values (ζ potential, volume fraction of particles ϕ, and electrolyte concentration relative to particle size, κa) and compared with other model approaches as well as with experimental data, with demonstrably good-to-excellent agreement found. The numerical package we have developed is robust and has been made available by the authors for general use.

As part of our ongoing efforts, we have investigated and quantified several transport properties in terms of electrokinetic linear response functions. In particular, we have focused attention on the dynamic mobility

$$\mu = \frac{2h(b)}{b}\left(1 + \phi\frac{\Delta\rho}{\rho_s}\right)^{-1} \tag{1}$$

expressed in terms of a hydrodynamic flow function h evaluated at the cell boundary ($r = b$). In the equation given above, $\Delta\rho = \rho_p - \rho_s$, where ρ_s and ρ_p are the mass densities of the fluid and particle, respectively.

More recently,[6] we quantified the complex conductivity, K^*, of a concentrated charged particle suspension based on the linear

(1) O'Brien, R. W. *J. Colloid Interface Sci.* **1986**, *113*, 81.
(2) O'Brien, R. W. *J. Fluid Mech.* **1988**, *190*, 71.
(3) O'Brien, R. W. *J. Fluid Mech.* **1990**, *212*, 81.
(4) Ahualli, S.; Delgado, A.; Miklavcic, S.; White, L. R. *Langmuir* **2006**, *22*, 7041.
(5) Ahualli, S.; Delgado, A.; Miklavcic, S.; White, L. R. *J. Colloid Interface Sci.* **2007**, *309*, 342.
(6) Bradshaw-Hajek, B. H.; Miklavcic, S. J.; White, L. R. *Langmuir* **2008**, *24*, 4512.
(7) Ohshima, H. *J. Colloid Interface Sci.* **1997**, *195*, 137.
(8) Ohshima, H. *J. Colloid Interface Sci.* **1997**, *188*, 481.
(9) Dukhin, A. S.; Shilov, V. N.; Borkovskaya, Y. B. *Langmuir* **1999**, *15*, 3452.
(10) Dukhin, A. S.; Shilov, V. N.; Ohshima, H.; Goetz, P. J. *Langmuir* **1999**, *15*, 6692.
(11) Lee, E.; Chu, J. W.; Hsu, J. *J. Colloid Interface Sci.* **1999**, *209*, 481.
(12) Hsu, J. P.; Lee, E.; Yen, F. Y. *J. Chem. Phys.* **2000**, *112*, 6404.
(13) Carrique, F.; Arroyo, F. J.; Delgado, A. V. *J. Colloid Interface Sci.* **2001**, *243*, 351.
(14) Carrique, F.; Arroyo, F. J.; Jimenez, M. L.; Delgado, A. V. *J. Chem. Phys.* **2003**, *118*, 1945.
(15) Zholkovskij, E. K.; Masliyah, J. H.; Shilov, V. N.; Bhattacharjee, S. *J. Colloid Interface Sci.* **2007**, *133−134*, 279.
(16) Bradshaw-Hajek, B. H.; Miklavcic, S. J.; White, L. R. *Langmuir* **2009**, *25*, 1961.

response formula $\mathbf{i} = K^*\mathbf{E}$. Using the self-consistent cell model, we deduced the complex conductivity to be

$$K^* = -\rho_{ch}^{(0)}(b)\mu\phi\frac{\Delta\rho}{\rho_s} + \sum_{j=1}^{N}\frac{z_j^2e^2n_j^{(0)}(b)}{\lambda_j}\frac{d\phi_j}{dr}(b)\exp\left[\frac{-z_je\Psi^{(0)}(b)}{k_BT}\right] + i\omega\varepsilon_s\varepsilon_0\frac{d\psi}{dr}(b) \quad (2)$$

where e, ε_s, ε_0, k_B, and T are the electron charge, the relative fluid dielectric permittivity, the vacuum permittivity, the Boltzmann constant, and the temperature, respectively. In addition z_j and λ_j are the valency and drag coefficient of the jth ion type (j = 1, 2, ..., N), respectively. The equilibrium electrostatic potential within the cell is denoted $\Psi^{(0)}(r)$, and $\psi(r)$ and $\phi_j(r)$ are perturbations to the electrostatic and electrochemical potentials, respectively, resulting from the application of the field. The equilibrium ion density $n_j^{(0)}$ and charge density $\rho_{ch}^{(0)}$ are given by

$$n_j^{(0)}(r) = n_j^{\infty}\exp[-z_je\Psi^{(0)}(r)/k_BT]$$

and

$$\rho_{ch}^{(0)}(r) = \sum_{j=1}^{N} z_jen_j^{(0)}(r)$$

where n_j^{∞} is the (reservoir) ion density.

From this, the experimental observable $\Delta K^*(\omega,\phi) = K^* - K_{sol}^*$, representing the departure of the complex conductivity (eq 2) from the bulk conductivity

$$K_{sol}^* = \sum_{j=1}^{N}\frac{z_j^2e^2n_j^{\infty}}{\lambda_j} - i\omega\varepsilon_s\varepsilon_0$$

can be determined. The real part of this difference defines the conductivity increment, while the imaginary part defines the dielectric permittivity increment[6]

$$\Delta\varepsilon'(\omega,\phi) = \frac{-\mathrm{Im}[\Delta K^*(\omega,\phi)]}{\omega\varepsilon_0} \quad (3)$$

In ref 6, these quantities were studied extensively as functions of frequency, ω, ζ potential, volume fraction of particles, ϕ, and electrolyte concentration for a wide range of values and compared with experiment.[16]

What has become clear from our investigations is the heavy reliance on a numerical solution of the system of complex ordinary differential equations for any form of quantitative analysis. In addition, it was noted in ref 16 that the dielectric permittivity is strikingly independent of particle surface charge and other double-layer properties of the system at high frequencies. The ionic diffusion length and hydrodynamic penetration depth were shown to be small compared with the size of the particle, reflecting the fact that changes in the field variables (velocity, electrostatic potential, charge density, etc.) occurred in a thin boundary layer near the particle surface. The physical implications of this boundary layer have been discussed in greater detail in refs 17 and 18.

Two questions arise naturally from these outcomes. First, how accurate are the numerical results of the simulations, especially at high frequencies where the differential equations become very stiff (i.e., near-singular)? Second, what possibility to extract simple but accurate closed formulas for the observed transport quantities exists and can be used to compare with experimental measurements, and what is the range of validity of such formulas? This paper seeks to address both questions through a matched asymptotic analysis of the complex differential equation system based on a high-frequency perturbation parameter, ϵ, arising naturally in the system. Other authors have utilized asymptotic and other techniques to examine the behavior of suspensions under limiting conditions of various system parameters. References 7, 19, and 20 studied the behavior of the dynamic mobility of suspensions at low ζ potential, while others[1,21,22] have studied the behavior of thin double-layer systems. Reference 7 also examined the case of zero relative particle dielectric permittivity.

We provide some answers to the preceding questions in section 4 of this paper by comparing high-frequency asymptotic approximations of the dynamic mobility, conductivity, and dielectric permittivity, derived in section 3, with full numerical simulations. Section 3 outlines the derivation of the inner and outer expansions of the linear response funtions valid inside and outside a boundary layer of thickness of order ϵ, respectively. We also detail the method employed to match these solutions at the extreme of the boundary layer. In section 2, we summarize the relevant equations and boundary conditions for the cell model of electrokinetics.

2. Governing Equations

Assuming a weak applied field $\mathbf{E}$ and linear electrokinetic response, the deviations from equilibrium behavior of the fluid velocity, electric potential, ion distributions, ion velocities, etc., are represented by functions that are dependent only on the radial distance from the particle surface multiplied by an angular factor accounting for the breaking of spherical symmetry.[1−3] That is, the electrokinetic quantities of interest are made up of an equilibrium contribution plus a linear response

$$\Xi(\mathbf{r},t) = \Xi^{(0)}(\mathbf{r}) + \xi(r)\mathbf{E}\cdot\hat{\boldsymbol{r}}e^{-i\omega t} + O[\mathbf{E}(t)^2] \quad (4)$$

In eq 4, $\Xi^{(0)}$ represents the field-independent, equilibrium contributions of the system properties, including the electric potential, the electrochemical potentials of the ions, and the pressure. In the second term, $\xi(r)$ represents any of the functions, $\psi(r)$, $\phi_j(r)$, and $P(r)$, which correspond to perturbations in the electrostatic potential, electrochemical potential, and hydrodynamic pressure. The perturbed fluid velocity, $\mathbf{u}$, resulting from the application of an external field takes the form (in the reference frame of the central particle)[23]

$$\mathbf{u}^{(1)}(\mathbf{r}) = (u_r, u_\theta, u_\phi) = \mu(\omega)\mathbf{E} - \left\{\frac{2h(r)}{r}\mathbf{E}\cdot\hat{\boldsymbol{r}}, \frac{1}{r}\frac{\partial[rh(r)]}{\partial r}(\mathbf{E}-\mathbf{E}\cdot\hat{\boldsymbol{r}}\hat{\boldsymbol{r}})\cdot\hat{\theta}, 0\right\}$$

(17) Hill, R. J.; Saville, D. A.; Russel, W. B. *Phys. Chem. Chem. Phys.* **2003**, *5*, 911.
(18) Ennis, J.; White, L. R. *J. Colloid Interface Sci.* **1996**, *178*, 460.
(19) Mangelsdorf, C. S.; White, L. R. *J. Colloid Interface Sci.* **1993**, *160*, 275.
(20) Ennis, J.; White, L. R. *J. Colloid Interface Sci.* **1996**, *178*, 460.
(21) Shilov, V. N.; Delgado, A. V.; Gonzalez-Caballero, F.; Grosse, C. *Colloids Surf., A* **2001**, *192*, 253.
(22) Ohshima, H. *Langmuir* **2005**, *21*, 9818.
(23) Landau, L. D.; Lifshitz, E. M. *Fluid Mechanics*; Pergamon Press: Oxford, U. K., 1966.

where $\mu(\omega)$ is the electrophoretic mobility and $h(r)$ is the hydrodynamic function appearing in eq 1.

With this linear response formulation, the electrokinetic problem in the presence of an oscillating field is reduced to solving within the cell, the following coupled set of complex ordinary differential equations for the above linear response functions ψ, ϕ_j, and h:[1]

$$\hat{L}\psi(r) = \frac{e^2}{\varepsilon_s\varepsilon_0 k_B T}\sum_{j=1}^{N} z_j^2 n_j^{(0)}(r)[\phi_j(r) + \psi(r)]$$

$$\hat{L}\phi_j(r) + \gamma_j^2[\phi_j(r) + \psi(r)] = \frac{e}{k_B T}\frac{d\Psi^{(0)}}{dr}(r)\left[z_j\frac{d\phi_j(r)}{dr} - \frac{2\lambda_j}{e}\frac{h(r)}{r}\right]$$

$$\hat{L}(\hat{L} + \gamma^2)h(r) = -\frac{e^2}{\eta_s k_B T}\frac{1}{r}\frac{d\Psi^{(0)}}{dr}\sum_{j=1}^{N} z_j^2 n_j^{(0)}(r)\phi_j(r)$$

with complex constants

$$\gamma = \frac{1+i}{\sqrt{2}}\sqrt{\frac{\omega\rho_s}{\eta_s}},\ \gamma_j = \frac{1+i}{\sqrt{2}}\sqrt{\frac{\omega\lambda_j}{k_B T}}$$

and the second-order differential operator

$$\hat{L} = \frac{d^2}{dr^2} + \frac{2}{r}\frac{d}{dr} - \frac{2}{r^2}$$

Here, η_s is the fluid viscosity.

This system must satisfy the following boundary conditions. At the particle surface, $r = a$

$$h(a) = \left.\frac{dh}{dr}\right|_{r=a} = 0$$

$$\left.\frac{d\phi_j}{dr}\right|_{r=a} = 0$$

$$\left.\frac{d\psi}{dr}\right|_{r=a} - \frac{\varepsilon_p}{\varepsilon_s a}\psi(a) = 0$$

where ε_p is the permittivity of the particle. At the cell boundary, $r = b$

$$\psi(b) = -b$$

$$\phi_j(b) = b$$

$$\left.\frac{d}{dr}\left[(\hat{L} + \gamma^2)h\right]\right|_{r=b} = \frac{\gamma^2 h(b)}{b}\frac{1 - \phi\frac{\Delta\rho}{\rho_s}}{1 + \phi\frac{\Delta\rho}{\rho_s}} + \frac{\rho_{ch}^{(0)}(r)}{\eta_s}$$

The equilibrium electrostatic potential $\Psi^{(0)}(r)$ satisfies

$$\frac{1}{r^2}\frac{d}{dr}\left[r^2\frac{d\Psi^{(0)}(r)}{dr}\right] = \begin{cases} 0 & r < a \\ -\dfrac{e}{\varepsilon_s\varepsilon_0}\displaystyle\sum_{j=1}^{N} z_j n_j^{(0)}(r) & a < r < b \end{cases}$$

subject to the following conditions. At the slipping plane at each particle surface, $r = a$

$$\Psi^{(0)}|_{r=a} = \zeta$$

while global electroneutrality leads to the condition

$$\left.\frac{d\Psi^{(0)}}{dr}\right|_{r=b} = 0$$

at the cell boundary, $r = b$.

Following ref 18, we define the dimensionless parameter ε as

$$\epsilon^2 = \frac{\kappa^2 k_B T}{\omega\bar{\lambda}}$$

where $\bar{\lambda}$ is as the average drag coefficient of the ions (as yet undefined). Debye screening length κ^{-1} is given by

$$\kappa^2 = \sum_{j=1}^{N}\frac{e^2 z_j^2 n_j^{\infty}}{\varepsilon_s\varepsilon_0 k_B T}$$

The parameter ϵ is the ratio between the ionic drift length and the Debye length. At the high frequencies of interest in this paper, $\epsilon \ll 1$. In section 4, we deduce high-frequency approximations for the conductivity, permittivity, and mobility, starting from the cell model equations given above, using the technique of matched asymptotic expansions based on this small parameter.

In scaled form, the equations for linear electrokinetics are[4]

$$\begin{cases} L\Psi - \sum_j \beta_j e^{-z_j Y(x)}(\Psi + \Phi_j) = 0, \\ L\Phi_j - \dfrac{L_j}{\epsilon^2}(\Psi + \Phi_j) = \dfrac{dY}{dx}\left[z_j\dfrac{d\Phi_j}{dx} - 2m_j\dfrac{H}{x}\right], \\ LQ = -\dfrac{1}{x}\dfrac{dY}{dx}\displaystyle\sum_j \beta_j e^{-z_j Y(x)}\Phi_j, \\ LH - \dfrac{K}{\epsilon^2}H = Q \end{cases} \tag{5}$$

where $L = \hat{L}/\kappa^2$ is the nondimensional version of $\hat{L}$. Here, $x = \kappa r$ is the nondimensionalized radial coordinate, and $Y(x) = e\Psi^{(0)}(r)/k_B T$ is the nondimensionalized equilibrium electrostatic potential, satisfying

$$\frac{1}{x^2}\frac{d}{dx}\left(x^2\frac{dY}{dx}\right) = -\sum_{j=1}\alpha_j e^{-z_j Y(x)} \tag{6}$$

with

$$Y|_{x_a} = \bar{\zeta}, \qquad \left.\frac{dY}{dx}\right|_{x_b} = 0$$

where $\bar{\zeta} = e\zeta/k_B T$ is the reduced ζ potential.

$\Psi(x) = \kappa\psi(r)$ is the nondimensionalized perturbation to the electrostatic potential, $\Phi_j(x) = \kappa\phi_j(r)$ is the nondimensionalized electrochemical potential function, $H(x) = \kappa h(r)/\mu_0$ is the nondimensionalized flow field function, and the function $Q(x)$ is defined by the last equation in eq 5. The nondimensional parameters are defined by

$$m_j = \frac{\lambda_j\mu_0}{e},\ \alpha_j = \frac{z_j n_j^{\infty}}{\sum_j z_j^2 n_j^{\infty}},\ \beta_j = z_j\alpha_j$$

where $\mu_0 = \varepsilon_s\varepsilon_0/\eta_s \times k_B T/e$. We have also introduced the new parameters

$$L_j = -i\frac{\lambda_j}{\bar{\lambda}},\ K = -i\frac{\rho_s k_B T}{\bar{\lambda}}\eta_s$$

In scaled form, the boundary conditions can be written

$$\begin{cases} \left.\dfrac{d\Psi}{dx}\right|_{x_a} - \dfrac{\varepsilon_p}{\varepsilon_s x_a}\Psi|_{x_a} = 0, \\ \left.\dfrac{d\Phi_j}{dx}\right|_{x_a} = 0, \\ H|_{x_a} = 0, \\ \left.\dfrac{dH}{dx}\right|_{x_a} = 0 \end{cases} \tag{7}$$

at the particle surface, $x = x_a$. At the cell boundary, $x = x_b$

$$\begin{cases} \Psi|_{x_b} = -x_b, \\ \Phi_j|_{x_b} = x_b, \\ Q|_{x_b} + \dfrac{K}{\epsilon^2} H|_{x_b} = 0, \\ \left.\dfrac{\mathrm{d}Q}{\mathrm{d}x}\right|_{x_b} - \dfrac{Q|_{x_b}}{x_b}\left(\dfrac{1-\phi\dfrac{\Delta\rho}{\rho_s}}{1+\phi\dfrac{\Delta\rho}{\rho_s}}\right) = \sum_j \alpha_j e^{-z_j Y(x_b)} \end{cases} \tag{8}$$

In terms of the nondimensional variables described above, the dynamic mobility (eq 1) is found to be

$$\frac{\mu}{\mu_0} = \frac{2H(x_b)}{x_b}\left(1+\phi\frac{\Delta\rho}{\rho_s}\right)^{-1} \tag{9}$$

and the complex conductivity increment ($\Delta K^* = K^* - K^*_{sol}$) representing the departure from the bulk conductivity is

$$\begin{aligned} \Delta K^* = {} & \frac{\kappa^2\varepsilon_0\varepsilon_s k_B T\mu_0}{e}\left.\frac{\mathrm{d}^2 Y}{\mathrm{d}x^2}\right|_{x_b}\frac{H(x_b)}{x_b}\frac{2\phi\frac{\Delta\rho}{\rho_s}}{1+\phi\frac{\Delta\rho}{\rho_s}} \\ & + \kappa^2\varepsilon_0\varepsilon_s k_B T\sum_j\frac{\beta_j}{\lambda_j}\left[\left.\frac{\mathrm{d}\Phi_j}{\mathrm{d}x}\right|_{x_b} e^{-z_j Y(x_b)} - 1\right] \\ & + i\omega\varepsilon_0\varepsilon_s\left(\left.\frac{\mathrm{d}\Psi}{\mathrm{d}x}\right|_{x_b} + 1\right) \end{aligned} \tag{10}$$

The existence of the ϵ^{-2} term in the governing eqs 5 is further evidence that for small ϵ (large frequency, ω), there is a boundary layer near the particle surface, as discussed by Ennis and White,[18] where the functions change, not over the cell dimension, but on a length scale of order ϵ.

3. Asymptotic Analysis

3.1. Inner and Outer Solutions and Matching Process. We know from the numerical solution for the problem[4] that the mobility $\mu \sim 1/\omega$ for a large frequency. From eq 9, we see that $\mu \propto H(x_b)$, so that for a large ω, i.e., small ϵ, we expect $H \sim \epsilon^2$. The above boundary conditions then suggest the following parameter expansions

$$\begin{cases} \Psi \sim \Psi_0 + \epsilon\Psi_1 + \epsilon^2\Psi_2 + ..., \\ \Phi_j \sim \Phi_{jo} + \epsilon\Phi j_1 + \epsilon^2\Phi_{j2} + ..., \\ Q \sim Q_0 + \epsilon Q_1 + \epsilon^2 Q_2 + ..., \\ H \sim \epsilon^2 H_2 + \epsilon^3 H_3 + \epsilon^4 H_4 + ... \end{cases} \tag{11}$$

for $\epsilon \to 0$.

The matched asymptotic analysis involves determination of the approximate forms for these functions in the boundary layer region near the particles (the inner solution) and in the outer region of the cell (the outer solution). As is standard practice, the inner solution will be designed to satisfy the boundary conditions on the particle surface at $x = x_a$, while the outer solution satisfies the boundary conditions at the cell boundary ($x = x_b$). The two functional forms must then be matched in the overlapping region to determine uniquely the solution set that is valid in the entire region. We shall detail these stages of the calculations explicitly in the following sections.

To find the form of the solution valid near the cell boundary, we substitute eq 11 into eqs 5 and boundary conditions 7 and 8 and collect powers of ϵ. The outer solution function can be found by solving the resulting differential equations for $\Psi(x)$, $\Phi_j(x)$, $Q(x)$, and $H(x)$.

To determine the form of the solution valid near the particle surface, we magnify the boundary layer through the stretching transformation

$$z = \frac{x - x_a}{\epsilon}$$

For the sake of brevity, we denote the field variables by Θ, where Θ represents Ψ, Φ_j, or Q. The differential operator, L, operating on a function Θ

$$\Theta = \Theta_0 + \epsilon\Theta_1 + \epsilon^2\Theta_2 + \epsilon^3\Theta_3 + ...$$

is

$$\begin{aligned} L\Theta(z) = {} & \frac{1}{\epsilon^2}\Theta_0'' + \frac{1}{\epsilon}\left(\Theta_1'' + \frac{2}{x_a}\Theta_0'\right) \\ & + \epsilon^0\left(\Theta_2'' + \frac{2}{x_a}\Theta_1' - \frac{2z}{x_a^2}\Theta_0' - \frac{2}{x_a^2}\Theta_0\right) \\ & + \epsilon\left(\Theta_3'' + \frac{2}{x_a}\Theta_2' - \frac{2z}{x_a^2}\Theta_1' - \frac{2}{x_a^2}\Theta_1 + \frac{2z^2}{x_a^3}\Theta_0' + \frac{4z}{x_a^3}\Theta_0\right) \\ & + o(\epsilon^2) \end{aligned} \tag{12}$$

where the primes indicate differentiation with respect to z.

The inner solution, $\Theta^I(z)$, must be matched to the corresponding outer solutions, $\Theta^O(x)$, in a region near the particle surface corresponding to $x = x_a + \epsilon z$, where $z \gg 1$. To obtain $\Theta^O(x)$, we expand around $x = x_a$ using the Taylor series

$$\begin{aligned} \Theta^O(z) = {} & \Theta_0^O|_{x_a} + \epsilon\left(\Theta_1^O|_{x_a} + z\Theta_0^{O'}|_{x_a}\right) \\ & + \epsilon^2\left(\Theta_2^O|_{x_a} + z\Theta_1^{O'}|_{x_a} + \frac{1}{2}z^2\Theta_0^{O''}|_{x_a}\right) \\ & + \epsilon^3\left(\Theta_3^O|_{x_a} + z\Theta_2^{O'}|_{x_a} + \frac{1}{2}z^2\Theta_1^{O''}|_{x_a} + \frac{1}{6}z^3\Theta_0^O|_{x_a}\right) + ... \end{aligned} \tag{13}$$

This form of the solution must be matched to the large z form of the inner solution

$$\Theta^I(z) = \Theta_0^I|_{z\gg1} + \epsilon\Theta_1^I|_{z\gg1} + \epsilon^2\Theta_2^I|_{z\gg1} + \epsilon^3\Theta_3^I|_{z\gg1} + ... \tag{14}$$

Hence, the large z asymptotic behavior of Θ_n^I must be an nth-degree polynomial in z. Any nonpolynomial behavior in the inner solution must decay to zero asymptotically for large values of z. Similar considerations for H starting at ϵ^2 lead to the same conclusions.

3.2. Electrostatic and Electrochemical Potential Functions, Ψ and Φ_j. The differential equations for the inner solution are obtained by substituting eq 12 for the operator L and the series expansions 11 into eqs 5 and boundary conditions 7 and 8.

The equations for $\Psi_0^I(z)$, $\Psi_1^I(z)$, $\Psi_2^I(z)$, and $\Psi_3^I(z)$ deduced from this process are

$$\begin{cases} \Psi_0^{I''} = 0, \\ \Psi_1^{I''} = -\dfrac{2}{x_a}\Psi_0^{I'}, \\ \Psi_2^{I''} = \dfrac{2z}{x_a^2}\Psi_0^{I'} + \dfrac{2}{x_a^2}\Psi_0^I - \dfrac{2}{x_a}\Psi_1^{I'} + \sum_j \beta_j e^{-z_j Y(x_a)}\left(\Psi_0^I + \Phi_{j0}^I\right), \\ \Psi_3^{I''} = -\dfrac{2z^2}{x_a^3}\Psi_0^{I'} - \dfrac{4z}{x_a^3}\Psi_0^I + \dfrac{2z}{x_a^2}\Psi_1^{I'} + \dfrac{2}{x_a^2}\Psi_1^I - \dfrac{2}{x_a}\Psi_2^{I'} \\ \qquad + \sum_j \beta_j e^{-z_j Y(x)}\left(\Psi_0^I + \Phi_{j0}^I\right) \end{cases} \tag{15}$$

A self-consistent expansion of the boundary conditions leads to

$$\begin{cases} \Psi_0^{I'}|_{z=0} = 0, \\ \Psi_n^{I'}|_{z=0} = \dfrac{\varepsilon_p}{x_a \varepsilon_s} \Psi_{n-1}^{I}|_{z=0}, \quad n = 1, 2, \ldots \end{cases} \tag{16}$$

The following analogous equations hold for various orders of $\Phi_j^I(z)$

$$\begin{cases} \Phi_{j0}^{I''} - L_j \Phi_{j0}^{I} = L_j \Psi_0^{I}, \\ \Phi_{j1}^{I''} - L_j \Phi_{j1}^{I} = L_j \Psi_1^{I} + \left(z_j \dfrac{dY}{dx}\bigg|_{x_a} - \dfrac{2}{x_a} \right) \Phi_{j0}^{I'}, \\ \Phi_{j2}^{I''} - L_j \Phi_{j2}^{I} = L_j \Psi_2^{I} + \left(z_j z \dfrac{d^2 Y}{dx^2}\bigg|_{x_a} + \dfrac{2z}{x_a^2} \right) \Phi_{j0}^{I'} \\ \qquad + \dfrac{2}{x_a^2} \Phi_{j0}^{I} + \left(z_j \dfrac{dY}{dx}\bigg|_{x_a} - \dfrac{2}{x_a} \right) \Phi_{j1}^{I'} \end{cases} \tag{17}$$

and an expansion of the boundary conditions leads to

$$\Phi_{jn}^{I}|_{z=0} = 0, \quad n = 0, 1, \ldots \tag{18}$$

The solution of eqs 15 for $\Psi^I(z)$ (to the third order) subject to boundary conditions 16 and eqs 17 for the $\Phi_j^I(z)$ (to the second order) subject to boundary conditions 18 give

$$\begin{cases} \Psi_0^{I}(z) = c_1, \\ \Psi_1^{I}(z) = \dfrac{\varepsilon_p c_1}{\varepsilon_s x_a} z + c_2, \\ \Psi_2^{I}(z) = \dfrac{c_1}{x_a^2} \left(1 - \dfrac{\varepsilon_p}{\varepsilon_s} \right) z^2 + \dfrac{\varepsilon_p c_2}{\varepsilon_s x_a} z + c_3, \\ \Psi_3^{I}(z) = c_4 + \dfrac{\varepsilon_p}{\varepsilon_s x_a} \left(c_3 - c_1 \sum_j \dfrac{\beta_j}{L_j} e^{-z_j \bar{\xi}} \right) z + \dfrac{c_2}{x_a^2} \left(1 - \dfrac{\varepsilon_p}{\varepsilon_s} \right) z^2 \\ \qquad - \dfrac{4}{3} \dfrac{c_1}{x_a^3} \left(1 - \dfrac{\varepsilon_p}{\varepsilon_s} \right) z^3 - \dfrac{\varepsilon_p c_1}{\varepsilon_s x_a} \sum_j \dfrac{\beta_j}{L_j^{3/2}} e^{-z_j \bar{\xi}} e^{-\sqrt{L_j} z}, \\ \qquad \ldots \end{cases}$$

$$\begin{cases} \Phi_{j0}^{I}(z) = -\Psi_0^{I}(z), \\ \Phi_{j1}^{I}(z) = -\Psi_1^{I}(z) - \dfrac{\varepsilon_p c_1}{\varepsilon_s x_a} \dfrac{1}{\sqrt{L_j}} e^{-\sqrt{L_j} z}, \\ \Phi_{j2}^{I}(z) = -\Psi_2^{I}(z) + \dfrac{\varepsilon_p c_1}{\varepsilon_s x_a L_j} z_j \dfrac{dY}{dx}\bigg|_{x_a} \\ \qquad - \dfrac{1}{2\sqrt{L_j}} \dfrac{\varepsilon_p c_1}{\varepsilon_s x_a} \left(z_j \dfrac{dY}{dx}\bigg|_{x_a} - \dfrac{2}{x_a} \right) z e^{-\sqrt{L_j} z} \\ \qquad - \left[\dfrac{\varepsilon_p c_2}{\varepsilon_s x_a \sqrt{L_j}} + \dfrac{1}{2L_j} \dfrac{\varepsilon_p c_1}{\varepsilon_s x_a} \left(z_j \dfrac{dY}{dx}\bigg|_{x_a} - \dfrac{2}{x_a} \right) \right] e^{-\sqrt{L_j} z}, \\ \qquad \ldots \end{cases}$$

where c_1, c_2, c_3, and c_4 are constants.

The differential equations for the outer solutions $\Psi^O(x)$ and $\Phi_j^O(x)$ are found by substituting expansions 11 into governing eqs 5. The equations for $\Psi_0^O(x)$, $\Psi_1^O(x)$, $\Psi_2^O(x)$, and $\Psi_3^O(x)$ are

$$\begin{cases} L\Psi_0^O - \sum_j \beta_j e^{-z_j Y(x)} (\Psi_0^O + \Phi_{j0}^O) = 0, \\ L\Psi_1^O - \sum_j \beta_j e^{-z_j Y(x)} (\Psi_1^O + \Phi_{j1}^O) = 0, \\ L\Psi_2^O - \sum_j \beta_j e^{-z_j Y(x)} (\Psi_2^O + \Phi_{j2}^O) = 0, \\ L\Psi_3^O - \sum_j \beta_j e^{-z_j Y(x)} (\Psi_3^O + \Phi_{j3}^O) = 0 \end{cases} \tag{19}$$

An expansion of the boundary conditions leads to

$$\begin{cases} \Psi_0^{O'}|_{x=x_b} = -x_b, \\ \Psi_n^{O'}|_{x=x_b} = 0, \quad n = 1, 2, \ldots \end{cases} \tag{20}$$

The analogous equations for outer solutions Φ_j^O are

$$\begin{cases} \Phi_{j0}^O = -\Psi_0^O, \\ \Phi_{j1}^O = -\Psi_1^O, \\ L\Phi_{j0}^O - L_j \Phi_{j2}^O = L_j \Psi_2^O + z_j \dfrac{dY}{dx} \dfrac{d\Phi_{j0}^O}{dx} \end{cases} \tag{21}$$

and an expansion of the boundary conditions leads to

$$\begin{cases} \Phi_{j0}^O|_{x=x_b} = x_b, \\ \Phi_{jn}^O|_{x=x_b} = 0, \quad n = 1, 2, \ldots \end{cases} \tag{22}$$

The solutions of eqs 19 subject to boundary conditions 20 for $\Psi^O(x)$ (to the third order) and eqs 21 subject to boundary conditions 22 for $\Phi_j^O(x)$ (to the second order) are

$$\begin{cases} \Psi_0^O(x) = -(1 + d_1\phi)x + d_1 \dfrac{x_a^3}{x^2}, \\ \Psi_1^O(x) = -d_2 x \left[\phi - \left(\dfrac{x_a}{x} \right)^3 \right], \\ \Psi_2^O(x) = -(1 + d_1\phi) \dfrac{I_2(x)}{x^2} - 2d_1 x_a^3 x I_{-4}(x) + d_3 x \left[1 - \left(\dfrac{x_b}{x} \right)^3 \right], \\ \Psi_3^O(x) = d_4 x \left[1 - \left(\dfrac{x_b}{x} \right)^3 \right], \\ \qquad \ldots \end{cases}$$

$$\begin{cases} \Phi_{j0}^O(x) = -\Psi_0^O(x), \\ \Phi_{j1}^O(x) = -\Psi_1^O(x), \\ \Phi_{j2}^O(x) = -\Psi_2^O(x) - \dfrac{z_j}{L_j} \dfrac{dY}{dx} \left(1 + d_1\phi + 2d_1 \dfrac{x_a^3}{x^3} \right) \\ \qquad \ldots \end{cases}$$

where d_1, d_2, d_3, and d_4 are constants and

$$I_n(x) = \int_x^{x_b} dx\, x^n \sum_j \frac{\beta_j}{L_j} e^{-z_j Y(x)}$$

By matching the orders of ε in eqs 13 and 14 for both Ψ and the Φ_j, we can solve for constants c_1, c_2, c_3, d_1, d_2, and d_3. We find

$$d_1 = \frac{-\left(1 - \frac{\varepsilon_p}{\varepsilon_s}\right)}{2 + \phi + (1 - \phi)\frac{\varepsilon_p}{\varepsilon_s}}$$

$$c_1 = \frac{-3x_a}{2 + \phi + (1 - \phi)\frac{\varepsilon_p}{\varepsilon_s}}$$

$$d_2 = 0$$

$$c_2 = 0$$

$$d_3 = \frac{-(1 + d_1\phi)\left(2 + \frac{\varepsilon_p}{\varepsilon_s}\right) x_a^{-3} I_2(x_a) + 2d_1 \left(1 - \frac{\varepsilon_p}{\varepsilon_s}\right) x_a^3 I_{-4}(x_a)}{\frac{1}{\phi}\left[2 + \phi + (1 - \phi)\frac{\varepsilon_p}{\varepsilon_s}\right]}$$

$$c_3 = d_3 x_a \left(1 - \frac{1}{\phi}\right) - (1 + d_1\phi) x_a^{-2} I_2(x_a) - 2d_1 x_a^4 I_{-4}(x_a)$$

3.3. Flow Field Functions, Q and H. The differential equations for inner solutions $Q^{\mathrm{I}}(z)$ and $H^{\mathrm{I}}(z)$ are

$$\begin{cases} Q_0^{\mathrm{I}''} = 0, \\ Q_1^{\mathrm{I}''} = -\dfrac{2}{x_a} Q_0^{\mathrm{I}'}, \\ Q_2^{\mathrm{I}''} = \dfrac{2z}{x_a^2} Q_0^{\mathrm{I}'} + \dfrac{2}{x_a^2} Q_0^{\mathrm{I}} - \dfrac{2}{x_a} Q_1^{\mathrm{I}'} - \dfrac{1}{x_a} \dfrac{\mathrm{d}Y}{\mathrm{d}x}\Big|_{x_a} \sum_j \beta_j \mathrm{e}^{-z_j \bar{\zeta}} \Phi_{j0}^{\mathrm{I}} \end{cases} \tag{23}$$

$$\begin{cases} H_2^{\mathrm{I}''} - KH_2 = Q_0^{\mathrm{I}}, \\ H_3^{\mathrm{I}''} - KH_3 = Q_1^{\mathrm{I}} - \dfrac{2}{x_a} H_2^{\mathrm{I}'}, \\ H_4^{\mathrm{I}''} - KH_4 = Q_2^{\mathrm{I}} + \dfrac{2z}{x_a^2} H_2^{\mathrm{I}'} + \dfrac{2}{x_a^2} H_2^{\mathrm{I}} - \dfrac{2}{x_a} H_3^{\mathrm{I}'} \end{cases} \tag{24}$$

An expansion of the boundary conditions leads to

$$\begin{cases} H_n^{\mathrm{I}}|_{z=0} = 0, \quad n = 2, 3, ..., \\ H_n^{\mathrm{I}}|_{z=0} = 0, \quad n = 2, 3, ... \end{cases} \tag{25}$$

The solutions to eqs 23 and 24 subject to boundary conditions 25 for $Q^{\mathrm{I}}(z)$ and $H^{\mathrm{I}}(z)$ are

$$\begin{cases} Q_0^{\mathrm{I}}(z) = 0, \\ Q_1^{\mathrm{I}}(z) = c_5(1 - \sqrt{K}z), \\ Q_2^{\mathrm{I}}(z) = c_6 + K\left(-\dfrac{c_5}{x_a K} - \dfrac{c_6}{\sqrt{K}} - \dfrac{c_1}{x_a K^{3/2}} \dfrac{\mathrm{d}Y}{\mathrm{d}x}\Big|_{x_a} \sum_j \beta_j \mathrm{e}^{-z_j \bar{\zeta}} \right) z \\ \qquad\qquad + \left(\dfrac{c_5 \sqrt{K}}{x_a} + \dfrac{c_1}{2x_a} \dfrac{\mathrm{d}Y}{\mathrm{d}x}\Big|_{x_a} \sum_j \beta_j \mathrm{e}^{-z_j \bar{\zeta}} \right) z^2, \\ \quad ... \end{cases}$$

$$\begin{cases} H_2^{\mathrm{I}}(z) = 0, \\ H_3^{\mathrm{I}}(z) = -\dfrac{1}{K} Q_1^{\mathrm{I}}(z) + \dfrac{c_5}{K} \mathrm{e}^{-\sqrt{K}z}, \\ H_4^{\mathrm{I}}(z) = -\dfrac{1}{K} Q_2^{\mathrm{I}}(z) - \dfrac{c_1}{x_a K^2} \dfrac{\mathrm{d}Y}{\mathrm{d}x}\Big|_{x_a} \sum_j \beta_j \mathrm{e}^{-z_j \bar{\zeta}} \\ \qquad - \dfrac{c_5}{x_a K} z \mathrm{e}^{-\sqrt{K}z} + \left(\dfrac{c_6}{K} + \dfrac{c_1}{x_a K^2} \dfrac{\mathrm{d}Y}{\mathrm{d}x}\Big|_{x_a} \sum_j \beta_j \mathrm{e}^{-z_j \bar{\zeta}} \right) \mathrm{e}^{-\sqrt{K}z}, \\ \quad ... \end{cases}$$

where c_5 and c_6 are constants.

The differential equations for outer solutions $Q^{\mathrm{O}}(x)$ and $H^{\mathrm{O}}(x)$ are

$$\begin{cases} LQ_0^{\mathrm{O}} = -\dfrac{1}{x} \dfrac{\mathrm{d}Y}{\mathrm{d}x} \sum_j \beta_j \mathrm{e}^{-z_j Y(x)} \Phi_{j0}^{\mathrm{O}}, \\ LQ_1^{\mathrm{O}} = -\dfrac{1}{x} \dfrac{\mathrm{d}Y}{\mathrm{d}x} \sum_j \beta_j \mathrm{e}^{-z_j Y(x)} \Phi_{j1}^{\mathrm{O}}, \\ LQ_2^{\mathrm{O}} = -\dfrac{1}{x} \dfrac{\mathrm{d}Y}{\mathrm{d}x} \sum_j \beta_j \mathrm{e}^{-z_j Y(x)} \Phi_{j2}^{\mathrm{O}} \end{cases} \tag{26}$$

$$\begin{cases} H_2^{\mathrm{O}} = -\dfrac{1}{K} Q_0^{\mathrm{O}}, \\ H_3^{\mathrm{O}} = -\dfrac{1}{K} Q_1^{\mathrm{O}}, \\ H_4^{\mathrm{O}} = -\dfrac{1}{K} (Q_2^{\mathrm{O}} - LH_2^{\mathrm{O}}) \end{cases} \tag{27}$$

An expansion of the boundary conditions leads to

$$\begin{cases} Q_n^{\mathrm{O}}|_{x=x_b} = -KH_{n+2}^{\mathrm{O}}|_{x=x_b}, \quad n = 0, 1, ..., \\ \dfrac{\mathrm{d}Q_0^{\mathrm{O}}}{\mathrm{d}x}\Big|_{x=x_b} - \dfrac{Q_0^{\mathrm{O}}(x_b)}{x_b} \dfrac{1 - \phi \dfrac{\Delta\rho}{\rho_{\mathrm{s}}}}{1 + \phi \dfrac{\Delta\rho}{\rho_{\mathrm{s}}}} = \sum_j \alpha_j \mathrm{e}^{-z_j Y(x_b)}, \\ \dfrac{\mathrm{d}Q_n^{\mathrm{O}}}{\mathrm{d}x}\Big|_{x=x_b} - \dfrac{Q_n^{\mathrm{O}}(x_b)}{x_b} \dfrac{1 - \phi \dfrac{\Delta\rho}{\rho_{\mathrm{s}}}}{1 + \phi \dfrac{\Delta\rho}{\rho_{\mathrm{s}}}} = 0, \quad n = 1, 2, ... \end{cases} \tag{28}$$

The solutions to eqs 26 and 27 subject to boundary conditions 28 for $Q^{\mathrm{O}}(x)$ and $H^{\mathrm{O}}(x)$ are

$$\begin{cases} Q_0^{\mathrm{O}}(x) = d_5 F_1(x) - (1 + d_1\phi) \dfrac{\mathrm{d}Y}{\mathrm{d}x} + d_1 x_a^3 x J_{-4}(x), \\ Q_1^{\mathrm{O}}(x) = d_6 F_1(x), \\ Q_2^{\mathrm{O}}(x) = d_7 F_1(x) + x \displaystyle\int_x^{x_b} (Y' \Psi^{\mathrm{O}}{}_2 - Y'' \Psi_2^{\mathrm{O}}) \dfrac{\mathrm{d}x}{x^2}, \\ \quad ... \end{cases}$$

$$\begin{cases} H_2^{\mathrm{O}}(x) = -\dfrac{1}{K} Q_0^{\mathrm{O}}(x), \\ H_3^{\mathrm{O}}(x) = -\dfrac{1}{K} Q_1^{\mathrm{O}}(x), \\ H_4^{\mathrm{O}}(x) = -\dfrac{1}{K} Q_2^{\mathrm{O}}(x) - \dfrac{1}{K^2} \left\{ Y' \left[-(1 + d_1\phi) + d_1\phi \dfrac{x_b^3}{x^3} \right] \right. \\ \qquad \left. \displaystyle\sum_j \beta_j \mathrm{e}^{-z_j Y(x)} \right\}, \\ \quad ... \end{cases} \tag{29}$$

where d_5, d_6, and d_7 are constants, $Y' = \mathrm{d}Y/\mathrm{d}x$, $Y'' = \mathrm{d}^2Y/\mathrm{d}x^2$, and $\Psi_2^{\mathrm{O}'} = \mathrm{d}\Psi_2^{\mathrm{O}}/\mathrm{d}x$

$$J_n(x) = \int_x^{x_b} \mathrm{d}x\, x^n \sum_j \alpha_j \mathrm{e}^{-z_j Y(x)}$$

and

$$F_1(x) = x \left(1 + \frac{2\phi \frac{\Delta\rho}{\rho_{\mathrm{s}}}}{3 + \phi \frac{\Delta\rho}{\rho_{\mathrm{s}}}} \left(\frac{x_b}{x} \right)^3 \right)$$

By matching orders of ε in eqs 13 and 14 for both Q and H, we can solve for the constants c_5, c_6, d_5, d_6, and d_7. We find

$$d_5 = [F_1(x_a)]^{-1} \left[(1 + d_1\phi) \frac{\mathrm{d}Y}{\mathrm{d}x}\Big|_{x_a} - d_1 x_a^4 J_{-4}(x_a) \right]$$

$$c_5 = -\frac{1}{\sqrt{K}} \left[d_5 F_1(x_a) - (1 + d_1\phi) \frac{\mathrm{d}^2 Y}{\mathrm{d}x^2}\Big|_{x_a} + d_1 x_a^3 J_{-4}(x_a) - d_1 \sum_j \alpha_j \mathrm{e}^{-z_j \bar{\zeta}} \right]$$

$$d_6 = c_5 [F_1(x_a)]^{-1}$$

$$c_6 = -\frac{1}{\sqrt{K}} \left[d_6 F_1(x_a) + \frac{c_5}{x_a} + \frac{c_1}{x_a \sqrt{K}} \frac{\mathrm{d}Y}{\mathrm{d}x}\Big|_{x_a} \sum_j \beta_j \mathrm{e}^{-z_j \bar{\zeta}} \right]$$

$$d_7 = [F_1(x_a)]^{-1} \left[c_6 - x_a \int_{x_a}^{x_b} \left(Y' \Psi^{\mathrm{O}}{}_2 - Y'' \Psi_2^{\mathrm{O}} \right) \frac{\mathrm{d}x}{x^2} \right]$$

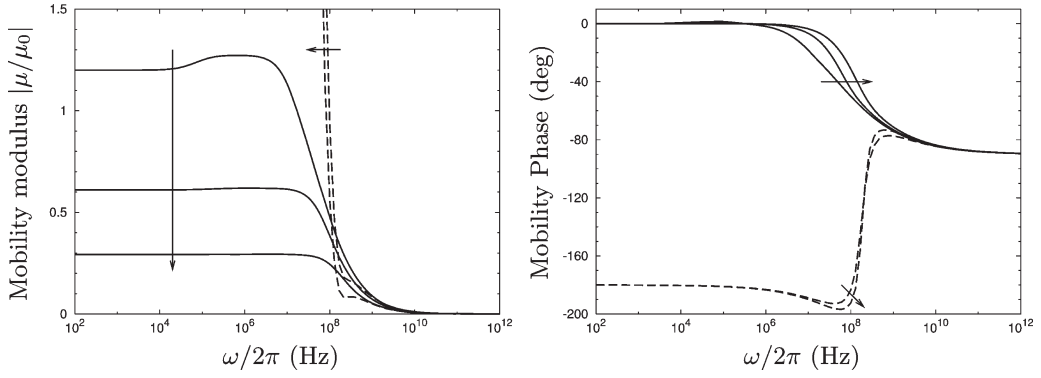

Figure 1. Frequency response of (left) the mobility modulus and (right) the mobility phase for ϕ values of 10^{-2}, 0.1, and 0.2. The solid lines show the full numerical solution, and the dashed lines show the high-frequency asymptotic expansion (only ϕ values of 10^{-2} and 0.2 are shown for the sake of clarity). Arrows show trends with increasing volume fractions. Reduced ζ potential is $\bar{\zeta} = 2$, and $\kappa a = 1$.

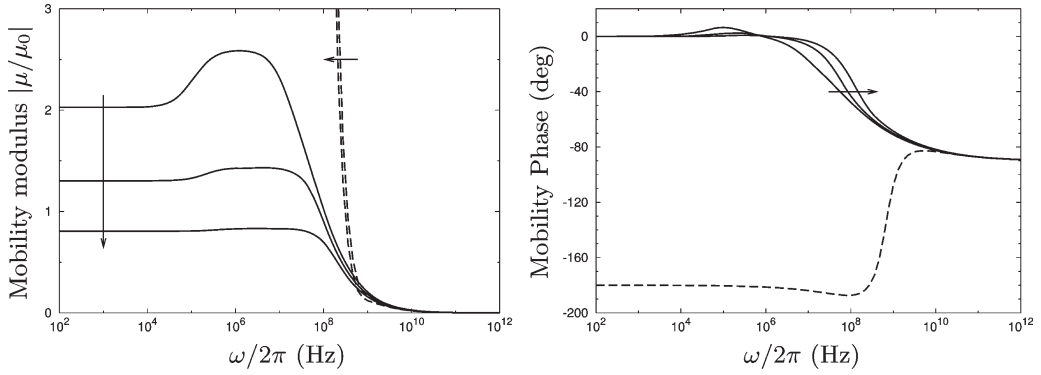

Figure 2. Like Figure 1, except $\bar{\zeta} = 4$ and $\kappa a = 1$. In the right panel, the high-frequency asymptotic expansions are indistinguisable for the various ϕ values.

The integral $\int_{x_a}^{x_b} (Y'\Psi_2^O - Y''\Psi_2^O)\,(dx/x^2)$ can be evaluated in terms of integrals over the solution of eq 6 for $Y(x)$ and the inner constants d_1 and d_3.

4. Comparison with Full Numerical Simulations

In this section, the high-frequency asymptotic forms for the dynamic mobility and the complex conductivity are compared with results obtained using the full numerical solution of the governing equations.

The figures in the following sections show that, with the exception of the dielectric permittivity, the high-frequency asymptotic expansions are valid only at frequencies beyond the current experimentally accessible range. For the case of an isolated particle, the high-frequency expansions derived in ref 18 were used to calculate the dynamic mobility and complex conductivity in high-frequency regimes where direct numerical solutions were not available. Padé approximants were used to extend the range of validity of the asymptotic expansions by matching the rational approximant with numerical data available at a lower frequency. Given that one aim of this paper is to write closed form solutions for the observable transport quantities, use of this technique is no longer appropriate. In this case, Padé approximants of the high-frequency expansions extend the range of validity only marginally and have therefore not been used.

In examining the accuracy of the high-frequency asymptotic expansions, we have found it sufficient to present comparisons at two different κa values, two different ζ potentials, and three different volume fractions.

4.1. Dynamic Mobility. By substituting the outer expansion for $H(x)$ (eq 29) into eq 9, we deduce the following asymptotic form for the dynamic mobility valid at high frequencies

$$\frac{\mu}{\mu_{0\epsilon\to 0}} = \frac{-6}{K\left(3+\phi\frac{\Delta\rho}{\rho_s}\right)}\epsilon^2(d_5+\epsilon d_6+\epsilon^2 d_7)+...$$

Note that since d_5 is real and K is imaginary, the leading order contribution to the dynamic mobility is purely imaginary. The second term makes both real and imaginary contributions.

Figures 1−4 show the frequency response of the dynamic mobility at increasing volume fractions for κa values of 1 and 5 and for reduced ζ potentials ($e\zeta/k_BT$) of 2 and 4. The solid lines show the full numerical cell model calculations,[4] and the dashed lines show the corresponding high-frequency asymptotic approximations. Left-hand panels show the mobility moduli, and right-hand panels show the phases.

One positive observation we can point out from the comparison is that in the high-frequency regime, the full numerical solution is indistinguishable from the high-frequency asymptotic solution for a wide range of κa values and ζ potentials. This indicates that the numerical solution is accurate even in a frequency range where the problem is numerically very stiff and where numerical solutions would be expected to be unreliable.

In terms of the usefulness of the asymptotic form as a quantitative tool, the figures show that the expansion is only accurate in the very high frequency regime. Via comparison of Figure 1 with Figure 3 and Figure 2 with Figure 4, this accuracy extends to slightly lower frequencies under low-κa (thick double layer) conditions. This should be anticipated since thick double-layer systems possess thinner boundary layers. At a fixed frequency, the expansion parameter, ϵ, which is a direct measure of the boundary layer

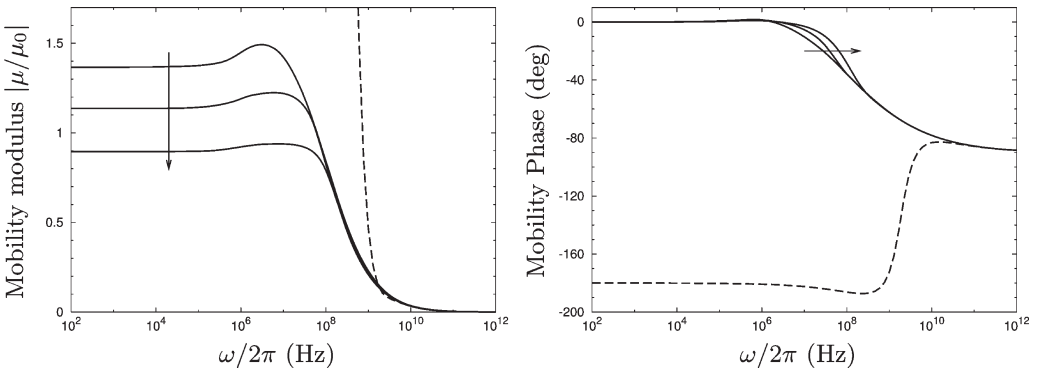

Figure 3. Like Figure 1, except $\bar{\zeta} = 2$ and $\kappa a = 5$. The high-frequency asymptotic expansions are indistinguisable for the various ϕ values.

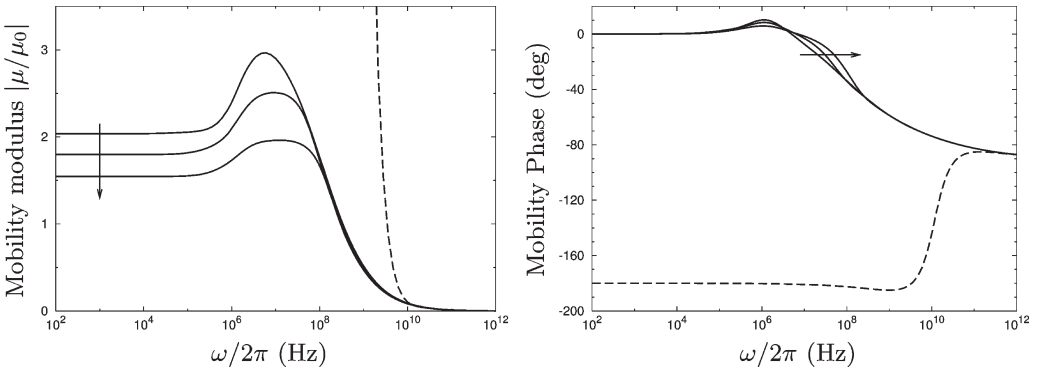

Figure 4. Like Figure 1, except $\bar{\zeta} = 4$ and $\kappa a = 5$. The high-frequency asymptotic expansions are indistinguisable for the various ϕ values.

thickness, decreases inversely with the extent of the double layer, κ^{-1}. It is therefore no surprise that we find improved agreement between the numerical and asymptotic results at lower κa values.

A less obvious outcome, reflected in the figures, is the suggestion that the high-frequency expansion of the dynamic mobility is accurate to lower frequencies for lower ζ potentials and is consistently a better approximation for the mobility modulus than for the phase.

4.2. Complex Conductivity. To exploit the fact that $\Phi_j = -\Psi$ at the zeroth and first orders in the expansion, it is convenient to rewrite eq 10 as

$$\Delta K^* = \frac{\kappa^2 k_B T \varepsilon_0 \varepsilon_s}{\bar{\lambda}} \left[\frac{\mu_0 \bar{\lambda}}{e} \frac{d^2 Y}{dx^2}\bigg|_{x_b} \frac{H(x_b)}{x_b} \frac{2\phi \frac{\Delta\rho}{\rho_s}}{1+\phi \frac{\Delta\rho}{\rho_s}} + \sum_j \frac{\beta_j e^{-z_j Y(x_b)}}{\lambda_j/\bar{\lambda}} \left(\frac{d\Psi}{dx}\bigg|_{x_b} + \frac{d\Phi_j}{dx}\bigg|_{x_b} - e^{z_j Y(x_b)} \right) - \frac{d\Psi}{dx}\bigg|_{x_b} + \frac{i}{\epsilon^2} \left(\frac{d\Psi}{dx}\bigg|_{x_b} + 1 \right) \right]$$

where $\bar{\lambda}$, given by

$$\bar{\lambda}^{-1} = \sum_j \frac{\beta_j}{\lambda_j} e^{-z_j Y(x_b)}$$

has been introduced here to affect the inclusion of the $d\Psi/dx$ term.

Since this expression involves system quantities evaluated only at the cell wall, only the outer expansions feature explicitly in the asymptotic form for ΔK^*. Substituting the outer expansions for $\Psi(x)$ and $H(x)$ [and implicitly $\Phi_j(x)$], we find that there are no contributions to the real part of the complex conductivity increment at orders ϵ^{-2} and ϵ^{-1}, while to order ϵ^0 the conductivity increment at high frequencies is

$$\mathrm{Re}(\Delta K^*)_{\epsilon \to 0} = \frac{\kappa^2 k_B T \varepsilon_0 \varepsilon_s}{\bar{\lambda}} \left(-\sum_j \frac{\beta_j}{\lambda_j/\bar{\lambda}} + 3id_3 \right) \qquad (30)$$

In contrast, there is a contribution at order ϵ^{-2} to the imaginary part of the complex conductivity but no contributions at orders ϵ^{-1} and ϵ^0. Since the dielectric permittivity increment is given by the imaginary part of the complex conductivity increment, as defined by eq 3, substitution of the outer expansions for $\Psi(x)$ and $H(x)$ gives the asymptotic form for the permittivity increment as

$$\Delta\varepsilon_{\epsilon \to 0} = 3\varepsilon_s d_1 \phi \qquad (31)$$

Unfortunately, neither eq 30 nor eq 31 exhibits any dependence on frequency. They therefore constitute limiting forms. To obtain higher-order terms would require determining the asymptotic forms for Φ_j and H to orders higher than ϵ^3.

Figures 5−8 show the frequency response of the complex conductivity increment at increasing volume fractions for two different κa values ($\kappa a = 1$ and 5) and two reduced ζ potentials ($e\zeta/k_B T = 2$ and 4). The solid lines refer to the results of the full numerical calculations, while the dashed lines show the corresponding high-frequency asymptotic limits (eqs 30 and 31). The real part of the conductivity increment is shown in the left-hand panels, and the dielectric permittivity is shown in the right-hand panels.

As one can anticipate from the preceding discussion, the agreement between the high-frequency asymptotic solution and the full numerical solution is limited to the high-frequency region

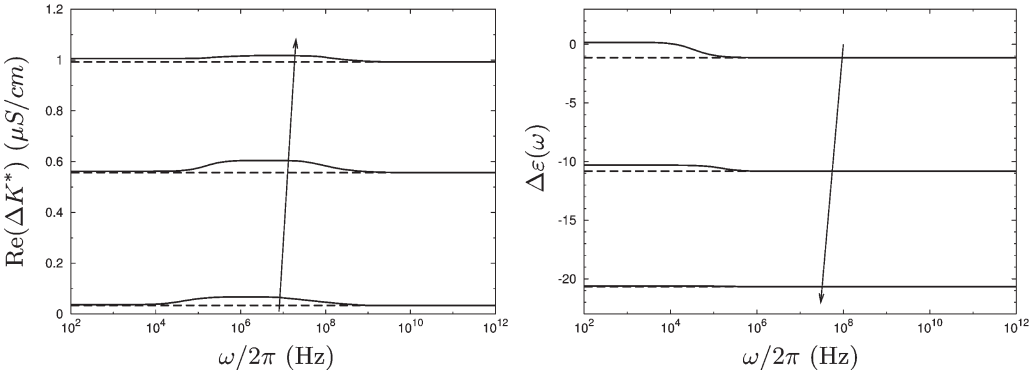

Figure 5. Frequency response of (left) the real part of the conductivity increment and (right) the dielectric permittivity increment for ϕ values of 10^{-2}, 0.1, and 0.2. The solid lines show the full numerical solution, and the dashed lines show the high-frequency asymptotic expansion. Arrows show trends with increasing volume fractions. The reduced ζ potential is $\bar{\zeta} = 2$, and $\kappa a = 1$.

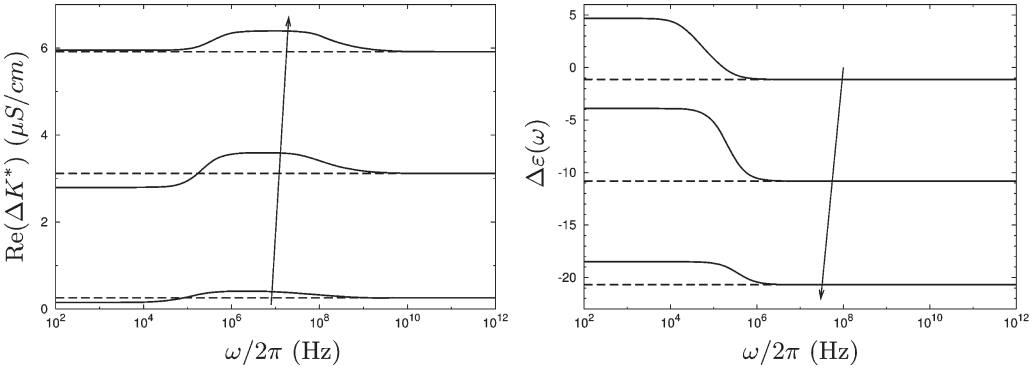

Figure 6. Like Figure 5, except $\bar{\zeta} = 4$ and $\kappa a = 1$.

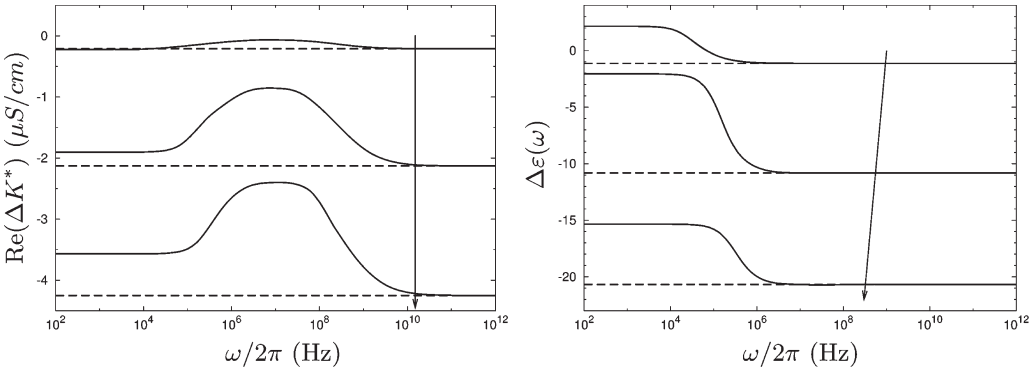

Figure 7. Like Figure 5, except $\bar{\zeta} = 2$ and $\kappa a = 5$.

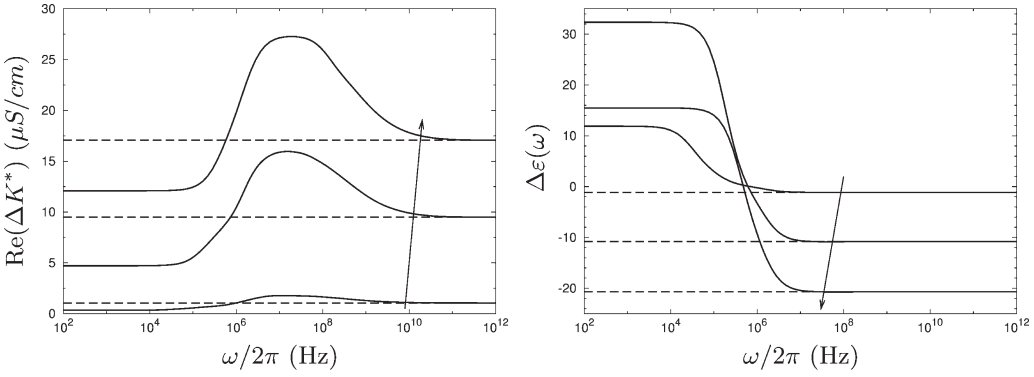

Figure 8. Like Figure 5, except $\bar{\zeta} = 4$ and $\kappa a = 5$.

where the problem is stiff. It is gratifying that the numerical scheme implemented here and in our previous works is so robust that it agrees with the analytic high-frequency limits under all double-layer conditions.

The high-frequency approximation for the real part of the complex conductivity increment shows the same trends with double-layer thickness and ζ potential as those exhibited by the dynamic mobility. Again, the high-frequency forms we have obtained are accurate at only very high frequencies, with slightly extended agreement for low κa and low ζ potential.

In contrast, our high-frequency form for the dielectric permittivity (eq 31) shows excellent agreement with the full numerical solution at frequencies down to the megahertz range. The approximation exhibts trends similar to the other measurable quantities with increasing ζ potentials and κa values: its accuracy at lower frequencies improves under low-ζ potential and low-κa conditions.

5. Final Remarks

The dynamic mobility and complex conductivity are measurable quantities that have the potential to be used to determine properties of particles in a colloidal system. It is therefore worthwhile to investigate the possibility of extracting analytic forms of these quantities to allow a more direct connection. In this paper, we have explored the high-frequency limits by the matched asymptotic method. The aims of this exploration, however, were 2-fold. We also sought closed form high-frequency formulas for these observable quantities to quantify the accuracy of the full numerical calculations at high frequencies where the system of governing equations becomes very stiff and where numerical approaches could be expected to break down.

With the numerical results for the complex conductivity, dielectric permittivity, and dynamic mobility exhibiting excellent agreement with the analytic, high-frequency asymptotic approximations, we have convincingly shown that the numerical method is accurate and robust under extreme conditions.

Our investigations have, moreover, shown that the high-frequency asymptotic formulas may be useful for directly calculating the dielectric permittivity in the megahertz range and above. For the other measurable physical quantities, the dynamic mobility and conductivity, full numerical calculations using a robust and accurate program, like the one used here and in our previous works, must be performed. Despite the appearance of a disappointing limitation of the asymptotic formulas to above the experimentally accessible range of frequencies, the result for the permittivity will provide useful information on which to base a detailed discussion of the dielectric response of the system.[24]

Finally, it is important to note that the results presented in this paper are valid even beyond the gigahertz range, provided the proper frequency-dependent dielectric responses of the particle and solvent molecules are considered.

(24) Bradshaw-Hajek, B. H.; Miklavcic, S. J.; White, L. R. Manuscript in preparation.